THE JOURNAL OF PHYSICAL CHEMISTRY C
A JOURNAL OF THE AMERICAN CHEMICAL SOCIETY

pubs.acs.org/JPCC

Article

# 1-Octanol Is a Functional Impurity Modifying Particle Size and Photophysical Properties of Colloidal ZnCdSSe/ZnS Nanocrystals

Seçil Sevim Ünlütürk, Ali Çağır, Canan Varlıklı, and Serdar Özçelik*

Cite This: *J. Phys. Chem. C* 2021, 125, 14401−14408

Read Online

ACCESS | Metrics & More | Article Recommendations | Supporting Information

**ABSTRACT:** Impurities in trioctylphophine (TOP) strongly affect nanocrystal synthesis. 1-Octanol among other contaminants in TOP is identified for the first time as a functional impurity by $^1$H NMR. The deliberate addition of 1-octanol into trioctylphosphine reduced particle size and modified photophysical properties of ZnCdSSe/ZnS colloidal nanocrystals. NMR analysis furthermore revealed that 1-octanol is bonded to the nanocrystal surfaces. The ratio of integrals for the O−$CH_2$ protons of 1-octanol, which is the lowest compared to the other ligands, suggests that 1-octanol plays a critical role to tune the particle size of nanocrystals. The increased amount of 1-octanol added into TOP reduces the particle size from 9.8 to 7.2 nm, causing a progressive blue shift in the UV−vis and PL spectra but leaving the alloy composition unaffected. The rate of nonradiative processes is enhanced with the amount of 1-octanol added into TOP, correlating with higher dislocation density observed in the nanocrystals. As a conclusion, 1-octanol is proposed as a functional impurity that varies particle size and nonradiative photophysical processes in the ZnCdSSe/ZnS colloidal nanocrystals.

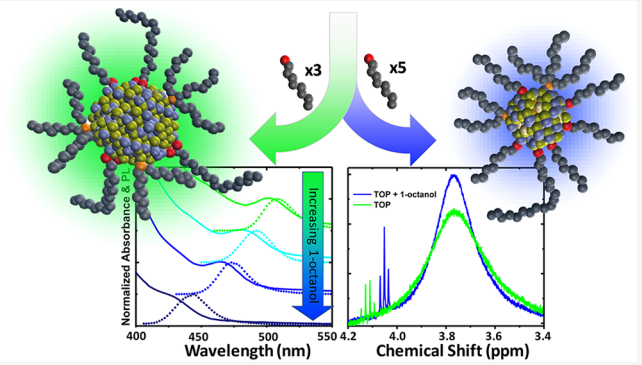


## INTRODUCTION

Colloidal nanocrystals (quantum dots) are mostly synthesized by the hot injection method.[1,2] Rapid injection of organometallic precursors in the presence of organic ligands is preferred because it promotes faster nucleation of nanocrystals and prevents their agglomeration. Ligands regulate nucleation and growth processes.[3] Phosphines bind strongly to nanocrystal surfaces and reduce nucleation and enhance growth rates while weakly binding ligands conversely operate on the rates. The nucleation and growth rates can be regulated by adjusting the molar ratio of ligands.[4] Some impurities in ligands were varying nanocrystal synthesis as well.[5] Composition[6] and structure[7] of nanocrystals and some photophysical properties[8] are controlled by the amount and type of ligands and impurities.

Impurities in trioctylphophine (TOP) and trioctylphophine oxide (TOPO) strongly changed synthesis and markedly modified the size, shape, and structure of nanocrystals.[8,9] The amount of impurity furthermore had an impact on the synthesis and the size and shape of nanocrystals.[9,10] Ligands having the same purity level but purchased from different vendors altered nucleation and growth rates and crystal morphologies.[9] Ligands with higher purity produce better morphology by slowing down reaction kinetics.[11]

Many phosphorus impurities in TOPO were identified and exploited to control the synthesis of colloidal CdSe quantum dots, rods, and wires.[10] Syntheses of nanocrystals in the presence of alkyl phosphonic acids arrange cadmium-rich surfaces due to stronger binding of phosphonate to cadmium.[6] Similarly, *n*-octylphosphonic acid and P,P′-(di-*n*-octyl) dihydrogen pyrophosphonic acid regulate the surface content of nanocrystals because they have a stronger affinity to cadmium atoms compared to TOPO.[12] Nuclear magnetic resonance (NMR) spectroscopy has been employed to identify impurities[13−16] and to distinguish the surface-bound ligands from the unreacted ones remaining in the medium.[17,18] Alcohols that are used to purify nanocrystals reduce photoluminescence (PL) quantum yields because alcohols are adsorbed to the nanocrystal surfaces.[17] Phenyldithiocarbamate creating a confinement barrier[19] changed the radiative decay rate.[20] Very recently, diphenylphosphine (DPP) was identified as a functional impurity regulating CdSe synthesis and doping level of manganese ions.[21] The controlled addition of DPP into TOP created a strong coupling between magnetic spins and excitons because a higher level of manganese doping was achieved in $Mn_xCd_{1-x}Se$ by the DPP addition.

While working on the synthesis of quaternary colloidal ZnCdSSe/ZnS nanocrystals, we noticed that TOP purchased

**Received:** February 24, 2021
**Revised:** June 1, 2021
**Published:** June 10, 2021

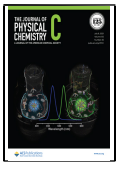






https://doi.org/10.1021/acs.jpcc.1c01676
*J. Phys. Chem. C* 2021, 125, 14401−14408

from two different vendors with different purity levels (97% and 90%) controlled the synthesis. Photoluminescent color and the particle size of the quaternary nanocrystals were tuned by the purity level of TOP used. $^1$H NMR spectroscopy is employed to identify impurity in TOP that strongly adjusted the particle size and emission color. 1-Octanol is identified among the other contaminants as the functional impurity that modified the nanocrystal synthesis. The controlled addition of 1-octanol into TOP (having 97% purity) regulated the particle size and altered the photophysical properties of the nanocrystals.

## METHODS

**Materials.** Cadmium acetate dihydrate ($Cd(Ac)_2{\cdot}2H_2O$, 98%), selenium powder (Se, 99.5%), sulfur powder (S, 99.98%), oleic acid (OA, 90%), 1-octadecene (ODE, 90%), trioctylphosphine (TOP, 97%), 1-octanol (99%), and solvents were purchased from Sigma-Aldrich. Zinc acetate dihydrate ($Zn(Ac)_2{\cdot}2H_2O$), zinc oxide (ZnO, 99.9%), and TOP (90%) were obtained from Alfa Aesar. Low and high purity TOP ligands are hereinafter referred to as TOP-LP and TOP-HP, respectively.

**Synthesis of ZnCdSSe/ZnS.** Colloidal ZnCdSSe/ZnS nanocrystals were synthesized by adopting a hot injection method.[22] Briefly, 0.14 mmol of $Cd(Ac)_2$ and 3.41 mmol of ZnO were dissolved in 7.0 mL of oleic acid (OA) at 150 °C in an inert atmosphere. The reaction temperature was increased to 300 °C after the addition of 15.0 mL of octadecene (ODE). Se-TOP and S-TOP were prepared by dissolving 2.20 mmol of Se and 2.20 mmol of S in 2.2 mL of TOP-HP individually at 300 °C. Predetermined amount (by keeping the total mole of ligands constant) of 1-octanol was added into S(Se)-TOP mixture to have different fractions of 1-octanol. S(Se)-TOP complexes were then rapidly injected into the cationic mixture at 300 °C to obtain the ZnCdSSe core nanoparticle. After 10 min, 1.6 mmol of S dissolved in 2.4 mL of ODE was added rapidly to the nanoparticle dispersion to form the ZnS shell layer on top of the core. Subsequently, the reaction temperature was reduced to 270 °C, and 2.86 mmol of $Zn(Ac)_2$ dissolved in 4.0 mL of OA and 1.0 mL of ODE, and 10.0 mmol of S dissolved in 5.0 mL of TOP-HP with 1-octanol were slowly and consecutively injected into the dispersion of core nanocrystals to form an additional ZnS layer. The reaction was quenched after 10 min of the latest injection by reducing the reactor temperature. For purification, the nanocrystal dispersions were diluted by hexane and precipitated by ethanol addition. The precipitated nanocrystals were separated by centrifugation at 6000 rpm for 20 min. The supernatant was emptied and the nanocrystals were redispersed in hexane to repeat the purification step. The particle synthesis with TOP-LP was the same except for 1-octanol addition.

**Instrumentation.** Absorption and photoluminescence spectra of the ZnCdSSe/ZnS nanocrystals were obtained by Edinburgh Instruments FS5 spectrophotometer. Absolute quantum yield measurements were carried out by using an integrated sphere accessory of the FS5 spectrophotometer. The time-correlated single-photon counting (TCSPC) technique was used to measure fluorescent lifetimes, using a laser at 365 nm. The particle size was measured by small-angle X-ray scattering (SAXS- Rigaku Ultima IV X-ray diffractometer) and verified by JEOL 2100F FEG high-resolution transmission electron microscope (HR-TEM). High-resolution TEM was used to image atomic arrangements. Compositional analysis of the particles was made by Philips XL 30S FEG scanning electron microscope equipped with energy dispersive X-ray spectroscopic (SEM-EDS) analyzer. XRD diffractograms were collected by Panalytical X'Pert Pro materials research diffractometer with Cu K$\alpha$ radiation ($\lambda$ = 1.5406 Å). $^1$H NMR spectra were measured by Varian VNMRJ 400 nuclear magnetic resonance spectrometer, and chemical shifts were calibrated by using the signal of $CDCl_3$ ($\delta$(H) = 7.26).

## RESULTS AND DISCUSSION

We noticed that the brand and purity level of TOP strongly influenced the absorption and emission wavelengths and consequently the photophysical properties of ZnCdSSe/ZnS nanocrystals. Although all the experimental parameters and the amounts of precursors were kept constant, TOP-LP resulted in nanocrystals having a blue emission at 470 nm, while TOP-HP led nanocrystals emitted at 518 nm (Figure 1). Since the purity

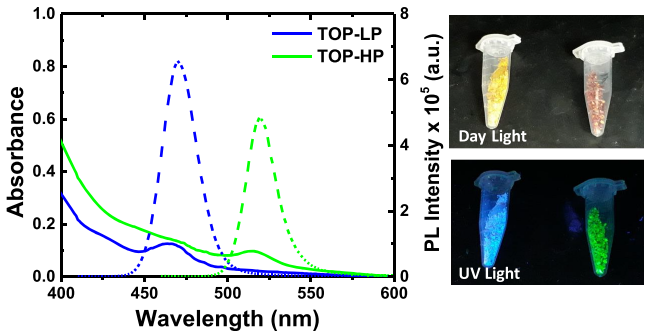


**Figure 1.** UV−vis absorption and photoluminescence (PL) spectra of ZnCdSSe/ZnS nanocrystals synthesized by using two different trioctylphosphine (TOP) brands having different purity levels. The blue-colored spectra belong to nanocrystals prepared in TOP-LP and the green-colored spectra obtained from nanocrystals synthesized in TOP-HP. All other experimental parameters and concentrations of precursors were kept constant. The powdery samples under daylight and UV light are shown on the right side of the figure.

level (proclaimed by the manufacturer) of TOP was different, NMR was used to verify purity levels of TOP and to identify impurities affecting the nanocrystal synthesis (Figure 2).

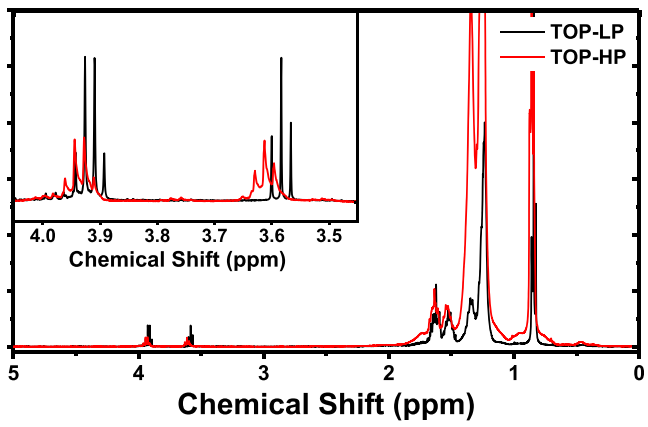


**Figure 2.** $^1$H NMR spectra of commercial trioctylphosphine with different levels of purities represented by black and red colors. The inset shows the impurity signals belonging to 1-octanol at 3.58 ppm and di-*n*-octylphosphinic acid at 3.92 ppm.



https://doi.org/10.1021/acs.jpcc.1c01676
J. Phys. Chem. C 2021, 125, 14401−14408

The $^1$H NMR spectra seen in Figure 2 display signals between 0.7 and 1.4 ppm originating from the protons of $CH_3$ and $CH_2$ groups of TOP and impurities with long carbon chains such as *n*-octyl-di-*n*-octylphosphinate (ODOP).[8] Furthermore, triplet and quartet signals were observed that may be originating from impurities in the TOP. The quartet at 3.92 ppm ($J$ = 6.7 Hz) indicates the presence of the P−O−$CH_2$ group of ODOP.[8] The triplet at 3.58 ppm ($J$ = 6.7 Hz) indicates the presence of the O−$CH_2$ group of 1-octanol. The signal intensities are correlated with the purity levels of TOPs. The $^1$H NMR spectra of TOP-HP/1-octanol mixtures with 1:1 and 10:1 mole ratios are given in Figure S1 as control analysis, which proves that the triplet signals stem from 1-octanol and varies with the fraction of 1-octanol. There are two likely explanations for the presence of 1-octanol: (i) hydrolysis of ODOP can release 1-octanol and di-*n*-octylphosphinic acid (DOPA) as side products, and (ii) poorer purification processes can favor the presence of 1-octanol as a side product formed by a radicalic reaction between 1-octene and water during the synthesis of TOP.[8] Despite ODOP, 1-octanol is not identified or mentioned in the literature as an impurity (except its impurity level) in TOP.[7] The integrated areas of $^1$H NMR spectra showed that TOP-LP contains 1.4-fold more 1-octanol and 1.8-fold more ODOP as impurity compared to TOP-HP for the same amount of TOP sample used.

NMR spectroscopy is frequently used to characterize the nature and structure of organic ligands as capping agents coating nanocrystal surfaces.[16] Figure 3 shows the $^1$H NMR spectra of the nanocrystals prepared with and without 1-octanol that is deliberately added into TOP-HP up to 1:1 mole ratio of samples prepared by 100 mg of purified nanocrystals dispersed in 700 $\mu$L of deuterated chloroform. Because the same amount of $CDCl_3$ was used in both samples, the relative intensity of protons belonging to $CHCl_3$ should be the same and can be used as the reference for quantitative analysis. Although the amounts of the nanocrystal samples were the same, the signal intensities in the 1:1 TOP/1-octanol mixture were higher compared to those in prepared TOP-only. The signal enhancement can be explained by the higher amount of 1-octanol bound to the increased surface area of the smaller nanocrystals. A higher amount of 1-octanol is required in the ligand mixture.

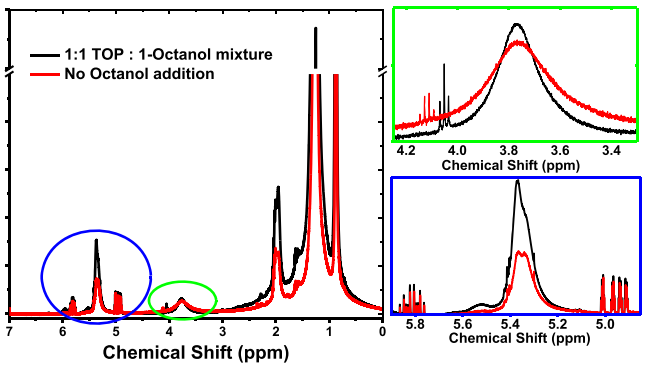


**Figure 3.** $^1$H NMR spectra of ZnCdSSe/ZnS nanocrystals prepared in the maximum amount (1:1 mol) of 1-octanol (black) and without 1-octanol (red) in the ligand mixture. Green and blue circled areas are enlarged to display the signals and their broadenings clearly. The broad signals indicate 1-octanols and oleic acid are bonded to the surfaces. The sharp triplet signal infers the remnant 1-octanols in the 1:1 mixture. The amount of 1-octanol remnant in the mixture is 20 times less compared to the bound ones.

The ligands we used in the synthesis are TOP, TOPO, oleic acid, and impurities like 1-octanol and DOPA that display $^1$H NMR signals in the aliphatic region (0.66−2.10 ppm). Therefore, the identification of these ligands bound to the surface of nanocrystals is arguable. However, the signals at more downfield regions are unique to identify ligands. The origin of broad signals in the $^1$H NMR spectrum is assigned to the surface bonded ligands since they slowly tumble on the surface of the nanocrystals. Broader signals appear in the downfield rather than the free ligands.[23] A comparison of the integrated peak areas provides the ratio of the $CH_2$ and $CH_3$ groups in the structure.[24] In both TOP-LP and TOP-HP samples, the ratio of $I_{CH2}/I_{CH3}$ was almost the same as 4.83 and 4.66, respectively. Integrals of the main peaks of the $^1$H NMR spectra are listed in Table 1. As mentioned above, the relative intensities of protons belonging to $CHCl_3$ impurity should be the same and can be used as a reference for the comparison of both spectra. The peaks at 0.96−0.76 ppm and 1.71−0.98 ppm were assigned to the protons in $CH_3$ and $(CH_2)_{n-1}$ in the alkyl chain of the ligands bonded to the nanocrystal. Similarly, the ratios of the integrals belonging to $CH_2$ to the integrals of $CH_3$ protons were calculated as 4.43 and 4.57 for the green- and blue-emitting nanocrystals, respectively. In both nanocrystals, ratios of integrals belonging to $CH_2$ and $CH_3$ groups were decreased compared to that of the commercially available TOP resources. The decreases in the integral ratios can be explained by the presence of 1-octanol, octadecene, and oleic acid on the surface of the nanocrystals.

As discussed above, Figure 3 clearly shows increased signal amplitudes originated by ligands around the surfaces of smaller nanocrystals. The integrals and their relative amount of change that belongs to these functional groups can be seen in Table 1. Interestingly the highest increment was observed for $CH_2$ and $CH_3$ groups that are present in the structures of almost all of our ligands. The amount of increase for the signals of oleic acid

**Table 1. Integrals of $^1$H NMR Spectra of the Blue- and Green-Emitting ZnCdSSe/ZnS Nanocrystals**

| compd | ppm | TOP only (green) | TOP/1-octanol (blue) | ratio[a] |
|---|---|---|---|---|
| chloroform | 7.27−7.25 | 1.00 | 1.00 | 1.00 |
| octadecene (ODE) | 5.87−5.75 | 1.13 | 1.57 | 1.39 |
| oleic acid (H−CR═CR−H) | 5.46−5.22 | 4.68 | 7.17 | 1.53 |
| octadecene (ODE) | 5.03−4.88 | 1.67 | 2.24 | 1.34 |
| 1-octanol (O−$CH_2$) | 3.95−3.53 | 6.56 | 8.00 | 1.22 |
| oleic acid ($CH_2$−C═X) | 2.10−1.81 | 10.72 | 16.70 | 1.56 |
| $CH_2$ | 1.71−0.98 | 73.91 | 128.76 | 1.74 |
| $CH_3$ | 0.96−0.76 | 14.26 | 23.90 | 1.68 |

[a]Area(TOP/1-octanol)/area(TOP).



https://doi.org/10.1021/acs.jpcc.1c01676
J. Phys. Chem. C 2021, 125, 14401−14408

was consistent (1.53 and 1.56) and greater compared to the increase of octadecene incorporation (1.39 and 1.34). The presence of a well-resolved $^1$H NMR signal and the absence of a broader peak for octadecene imply that it does not directly bind to the nanocrystal surfaces; instead, it was dissolved in the hydrophilic parts of the ligands around the nanocrystals. Because of the higher boiling point, it is difficult to remove octadecene by evaporation. Although it was stirred first with hexane which can dissolve octadecene better than ethanol (the precipitating agent in the purification step), and even after being purified twice, octadecene still existed in the samples. Finally, the broad signal at 3.95−3.53 ppm was interpreted as O−$CH_2$ protons for 1-octanol bonded to nanocrystal surfaces because a downfield chemical shift was expected for the ligands connected to nanocrystal structure as discussed in the literature.[23] The triplet signal, which comes from the 1-octanol, shifted to the downfield region compared to the $^1$H NMR spectrum of the TOP sample given in Figure 2. On the other hand, it is expected to observe a triplet signal rather than a broadened signal.[23] These 1-octanols are not directly bonded to the surface of the nanocrystals, but they are in the vicinity of the nanocrystal surface. The ratio of the integrals for O−$CH_2$ protons of 1-octanol is the lowest compared to those of other ligands which implies that 1-octanol plays a significant role to tune the particle size of the nanocrystals. Relative integrals belonging to O−$CH_2$ and $CH_2$−C═X protons indicated the presence of comparable amounts of 1-octanol and oleic acid bound to the nanocrystal surfaces.

On the basis of these findings, a set of experiments were conducted to explore the amount of 1-octanol addition to control the particle size and photophysical properties of the nanocrystals. For this purpose, the predetermined amount of 1-octanol (Sigma-Aldrich, 99%) was purposefully added into TOP-HP to increase the mole fraction of 1-octanol in the ligand mixture (as 1-octanol/TOP ratio varied 1.00, 0.28, 0.03, and 0.00 by keeping the total mole of ligands constant).

Absorption and photoluminescence (PL) spectra of ZnCdSSe/ZnS nanocrystals were shifted to blue more than 65 nm as the mole ratio of 1-octanol in TOP-HP was increased from 0.00 to 1.00 (Figure 4a). The PL maximum of the nanocrystal prepared in 0.28 mole ratio of TOP-HP/1-octanol matches the PL maximum of the nanocrystals synthesized in TOP-LP without 1-octanol addition (Figure 1). The fwhm values of PL spectra were approximately the same, 28 nm for all the samples. Furthermore, the Stokes shift is increased with a higher amount of 1-octanol added into TOP-HP (Table 2). But the quantum efficiency was decreased with a higher amount of 1-octanol added (Table 2 and Figure 4b inset). These findings suggest that 1-octanol acts as a functional additive/impurity that varies the photophysical properties of the ZnCdSSe/ZnS nanocrystals. The bandgap and the photophysical properties of nanocrystals can be modified by the particle size or chemical composition. The particle size is inversely proportional with the bandgap energy: (bandgap ≈ (1/mass of alloy) × particle size).[25−27] The composition analysis of the nanocrystals by SEM-EDS (Figure 5) validated that the chemical compositions of the alloyed nanocrystals were not varied with the amount of 1-octanol added into TOP-HP. The ratios of Zn−S−Cd−Se remained fixed. The nanocrystals had higher amounts of zinc and sulfur because substantial amounts of zinc and sulfur precursors were initially used to synthesize the core and to form the shell layers. As the amounts of 1-octanol added to TOP-HP were increased, the

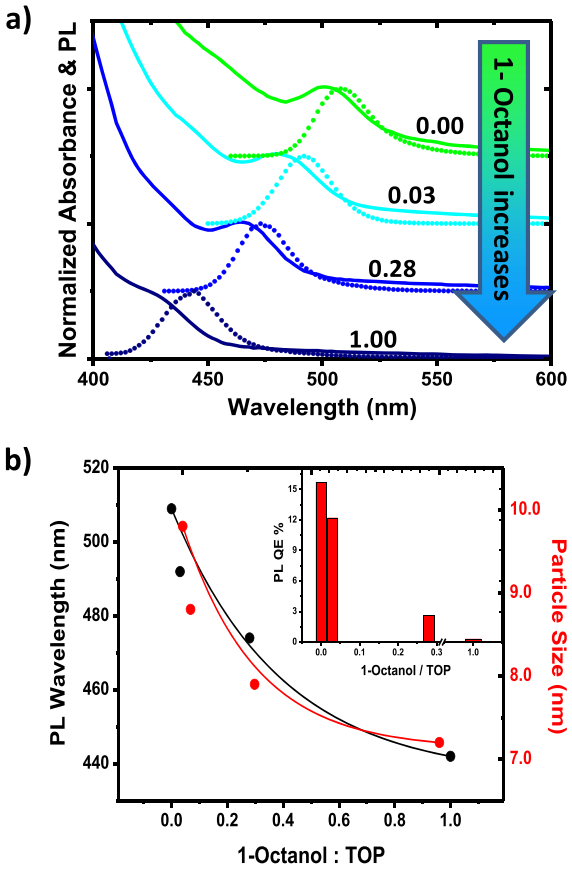


**Figure 4.** (a) UV−vis absorption and PL spectra of ZnCdSSe/ZnS nanocrystals prepared by increasing 1-octanol/TOP mole ratio while keeping other precursors and reaction parameters constant. From bottom to top 1-octanol/TOP mole ratio values are 1.00, 0.28, 0.03, and 0.00. (b) Blue shifting in PL wavelengths and the reduction of the particle size are correlated and controlled by the mole ratio of 1-octanol/TOP. The particle size data were obtained by SAXS measurements provided in Figure S2. The decrease in PL quantum efficiency (QE %) shown as an inset was proportional to the mole ratio of 1-octanol.

particle size was steadily decreased from 9.8 to 7.2 nm (Figure 4b). By combination of these findings, the blue-shift observed in the UV−vis and PL spectra is explained by the reduction in the particle size of the nanocrystal and suggests that *1-octanol controls the particle size and the bandgap of colloidal ZnCdSSe/ZnS nanocrystals*.

1-Octanol is identified and validated as a functional impurity to tune the particle size. Depending on the binding strength of the ligands, the particle size can be adjusted. The strong binding ligands like trioctylphosphine oxide (TOPO), TOP, and hexadecylamine (HDA) establish stable coordination complexes with $Cd(OOCR)_2$. It is called an "inhibited complex" that prevents the nucleation of the nanocrystals.[28] Especially at relatively lower reaction temperatures, below 200 °C, nanocrystals could not be formed because the inhibited complexes are present. Thiols, which are also classified as strong ligands, inhibit the nucleation process as well.[29] We used 1-octanethiol instead of 1-octanol to check this hypothesis, all other chemicals and reaction parameters were kept constant. The UV−vis absorption and PL spectra are given in Figure S3 and showed that there was a significant reduction in terms of PL intensity by 1-octanethiol addition. On the other hand, in the presence of relatively weaker ligands


https://doi.org/10.1021/acs.jpcc.1c01676
J. Phys. Chem. C 2021, 125, 14401−14408

**Table 2. Photophysical Properties of ZnCdSSe/ZnS Nanocrystals with Respect to the Amount of 1-Octanol Added into TOP-HP, as a Mole Ratio in the Ligand Mixture[a]**

| sample name | 1-octanol/TOP (mole ratio) | $\lambda_{Abs}$ (nm) | $\lambda_{PL}$ (nm) | fwhm (nm) | Stokes shift (nm) | particle size by SAXS (nm) | QE (%) (Int.Sph) | lifetime, $\tau_{average}$ (ns) |
|---|---|---|---|---|---|---|---|---|
| Oc-0 | 0.00 | 502 | 509 | 28 | 7 | 9.8 ± 1.98 | 15.7 | 15.6 |
| Oc-1 | 0.03 | 480 | 492 | 28 | 12 | 8.8 ± 2.04 | 12.2 | 16.1 |
| Oc-2 | 0.28 | 464 | 474 | 27 | 10 | 7.9 ± 1.79 | 2.6 | 12.0 |
| Oc-3 | 1.00 | 425 | 442 | 29 | 17 | 7.2 ± 1.56 | 0.3 | 9.3 |

[a]The average lifetimes, $\tau_{average}$, were calculated according to the equation given in Supporting information.

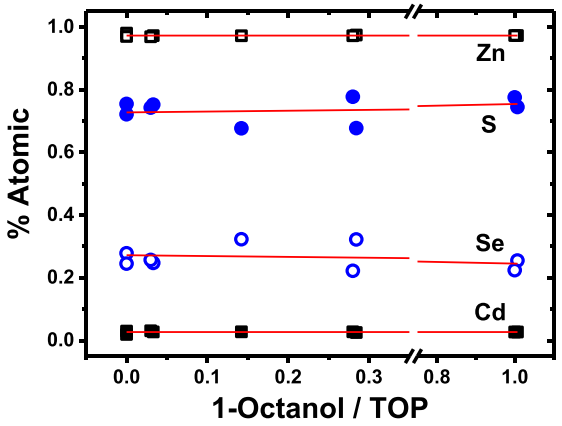


**Figure 5.** Elemental compositions of ZnCdSSe/ZnS alloyed nanocrystals prepared in TOP-HP with an increased amount of 1-octanol added. The atomic percent of each element is determined by SEM-EDS as the amount of 1-octanol increases. The red lines are guides for the eyes.

like fatty alcohols as in our case, the reaction prefers to form an "activated complex" of $Cd(OOCR)_2$ which could decompose into cadmium-complex monomers easily. In our case, 1-octanol as fatty alcohol is considered as a weaker ligand compared to TOP.

Besides cationic precursors as $Cd(OOCR)_2$, chalcogenide complexes like TOP-S and TOP-Se also affect the nucleation rate of the nanocrystals. Increasing the purity of TOP reinforces the bonds between phosphine and sulfur (selenium) in TOP-S (TOP-Se) complexes which decrease the reactivity of these reagents. No reaction occurs in the nucleation phase of the nanocrystals in ultrapure reagents because of the strong ligand interactions.[28] Strong binding complexes such as TOP-S and TOP-Se reduce the nucleation rate and delay particle formation. According to the LaMer model of the burst nucleation theory, the longer nucleation process results in the broad size distribution of the nanocrystals because some nuclei are already formed and grown while others are at the beginning to form seeds. If the nucleation process occurs rapidly, the faster nucleation and growth of nanocrystals may lead to a narrower size distribution.[30,31] In our case, when 1-octanol as a weak ligand was added, a shorter nucleation time leads to smaller nanocrystals formed, as demonstrated by the narrower size distribution provided in Figure S2.

Due to the fast nucleation time of the hot injection procedure, it is rather difficult to monitor the exact size of nuclei at higher reaction temperatures. However, regardless of the effect of the nucleation process on the particle size, a notable difference in the particle size was observed during the growth processes. Ostwald ripening theory which explains the growth mechanism of nanoparticles suggests that the large particles grow while the small ones dissolve. The key parameters are the reaction temperature, precursor ratio, and ligands. While higher reaction temperature provides higher activation energy for particle nucleation, the ligands facilitate the growth of the nanocrystals by altering the reaction environment.[32] In our system, the reaction temperature and the precursor ratio were kept constant. The only parameter varied is the ligand concentration which is effective in the Ostwald ripening mechanism. The 1-octanol/TOP mole ratio was adjusted, but the total mole of these ligands was kept constant. Since the Ostwald ripening mechanism results in broad size distribution, it is a challenge to have narrow particle size distributions.[33] In general, Ostwald ripening controls the growth of nanoparticles in a dispersion. The SAXS (Figure S2) and TEM (Figure 6) measurements suggest that the addition

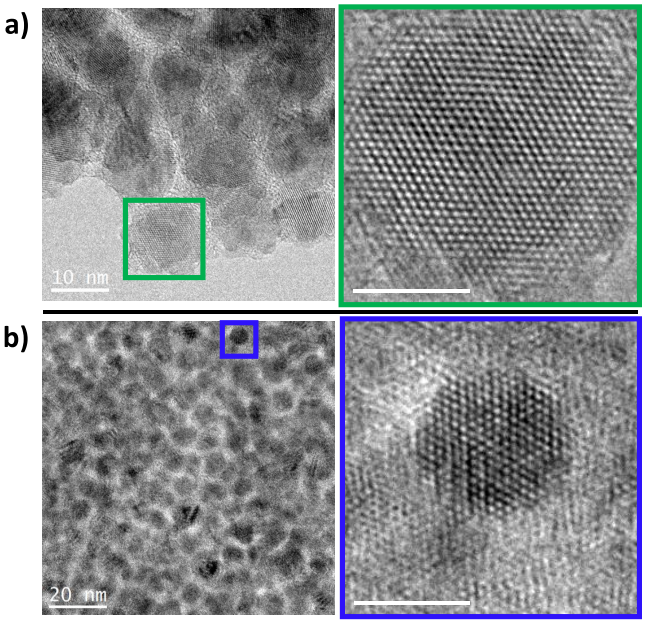


**Figure 6.** A high-resolution TEM image and detailed HRTEM image of the green squared (a) green-emitting nanocrystals prepared in TOP-HP without octanol addition and (b) blue-emitting nanocrystals prepared in TOP-HP with the ligand mixture of 1:1 TOP/1-octanol.

of 1-octanol keeps the particles smaller by slowing down nucleation and growth processes combined. The blue-emitting nanocrystals prepared in the presence of a higher amount of 1-octanol have a narrower size distribution compared to the green-emitting ones, prepared without 1-octanol addition. Convincingly, 1-octanol plays a significant role in both nucleation and growth phases to control the particle size and size distributions.

Table 2 summarizes the photophysical properties of colloidal ZnCdSSe/ZnS nanocrystals modified by the amount of 1-octanol added into TOP-HP. The PL lifetimes were fit to a



https://doi.org/10.1021/acs.jpcc.1c01676
J. Phys. Chem. C 2021, 125, 14401−14408

three-component exponential decay model in which the $\chi^2$ value was no longer reduced, and no systematic deviation was observed in the residuals. The slowest decay component ($\tau_3$ in Table S1) is assigned to exciton recombination on the nanocrystal surfaces. On the other hand, the faster process ($\tau_1$ in Table S1) is mainly attributed to the intrinsic exciton recombination in the core structure.[34] As shown in Table S1, the contribution of the slower process is reduced by the addition of 1-octanol as the exciton recombination on the nanocrystal surface was decreased. The radiative and nonradiative rate constants are determined by the equations provided in Supporting Information.[35,36] Figure 7 shows how

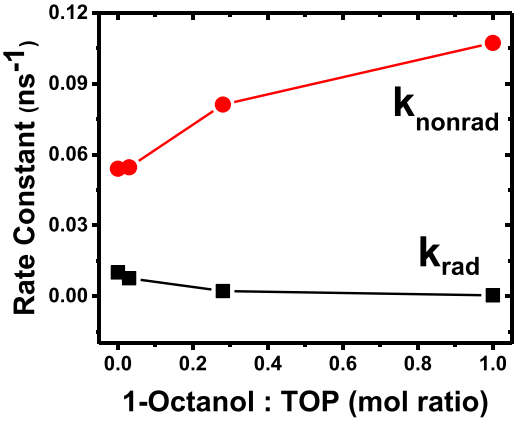


**Figure 7.** Radiative (black) and nonradiative (red) rate constants are varied by the mole ratio of 1-octanol/TOP. All the numerical values are given in Table S1.

the radiative and nonradiative rate constants varied with the 1-octanol added into TOP (Table S1). The nonradiative rate constants are increased with the amount of 1-octanol added; however, the radiative rate constants are almost unchanged. Understanding the exact photophysical mechanism related to the regulation of the rate constants is considerably complicated.[37] Therefore, we presume that the decrease in the quantum yield of the blue-emitting ZnCdSSe/ZnS nanocrystals is due to the significant increase in the nonradiative relaxations. The increased number of empty atomic spaces pointed out in Figure S4 suggested the formation of structural defects by the deliberate addition of 1-octanol. We inferred that the nonradiative processes are initiated by these structural defects formed by 1-octanol addition.[35] However, the radiative processes are not modulated by 1-octanol addition.

All these findings agree with NMR analysis that suggests that 1-octanols are adsorbed on the nanocrystal surface. Moreover, a significant decrease in the quantum yield and shortening of the lifetime (Table 2) indicate that the defects stimulate the nonradiative processes.

Dislocations in nanocrystal structures may enhance nonradiative recombinations.[38] Dislocation density (estimated by the equations given in Supporting Information) is related to the crystallite size.[39] The crystallite sizes were determined by the Scherrer equation using the XRD diffractograms (Figure 8).[40] The calculated crystallite sizes (the particle core size) for blue- and green-emitting nanocrystals are respectively 3.09 and 3.45 nm and agreed with TEM measurement that displays the whole nanocrystal but not able to distinguish the shell layer from the core crystallite. The dislocation densities for the blue-

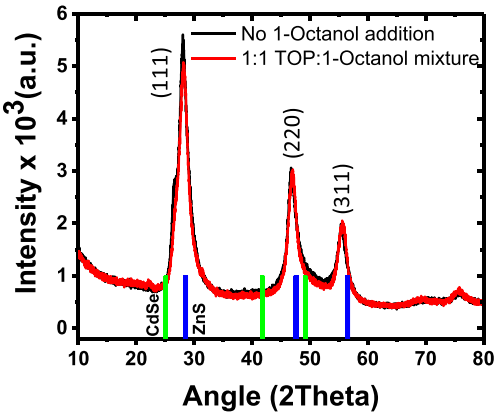


**Figure 8.** XRD diffractograms of ZnCdSSe/ZnS nanocrystals prepared in TOP-HP with and without 1-octanol addition. Reference lines for zinc blende bulk structures of CdSe and ZnS are given at the bottom of the patterns as green and blue vertical markers, respectively.

and green-emitting nanocrystals were calculated as $1.05 \times 10^{13}$ cm$^{-1}$ and $0.84 \times 10^{13}$ cm$^{-1}$, respectively. This calculation estimates about 20% increase in defect density and infers that the blue-emitting nanocrystals prepared in TOP-HP by the 1-octanol addition have higher dislocation density. HR-TEM images given in Figure S4 verify the increased number of void atomic spaces.

Figure 8 shows the XRD diffractograms of the nanocrystals prepared in TOP-HP with and without 1-octanol addition. Both samples displayed the same diffraction patterns having the same peak intensities. These diffractograms suggest that colloidal ZnCdSSe/ZnS nanocrystals possess the zinc blende cubic structure having three dominant diffraction peaks at Bragg angles of 30°, 48°, and 56°. These peaks are assigned to diffractions coming from the *hkl* facets of 111, 220, and 311 planes of the zinc blende structure. The XRD peak positions are between the CdSe and ZnS structural reference lines of bulk zinc blende crystal, indicating an alloyed crystalline structure. The XRD patterns validate the compositional analysis by SEM-EDX that showing the chemical composition of the nanocrystals prepared with and without 1-octanol addition is not changing. The diffraction peaks are closer to the ZnS lines which are consistent with a thicker ZnS layer formed on the nanocrystal surfaces (Figure 5, SEM_EDX analysis).

## CONCLUSION

We synthesized colloidal ZnCdSSe/ZnS nanocrystals by using two different TOPs with different purity levels (90% and 97% reported by the vendors Alfa Aesar and Sigma-Aldrich, respectively). 1-Octanol is identified as a functional impurity among other contaminants in TOP. The particle size is reduced as the amount of 1-octanol is deliberately increased, resulting in blue shifting in the UV−vis and PL spectra, but the chemical composition remained unchanged. NMR analysis suggested that 1-octanols are bonded to the nanocrystal surfaces. The increased amount of 1-octanol in TOP-HP created higher dislocation density, which led to enhanced nonradiative processes. The alloyed nanocrystals are rich in terms of zinc and sulfur but have very low cadmium content, less than 1%. Thus, this colloidal alloy may be considered as a low-toxic compound, alleviating the restriction on cadmium-containing materials that may be employed in display


https://doi.org/10.1021/acs.jpcc.1c01676
J. Phys. Chem. C 2021, 125, 14401−14408

technologies demanding high color purity (narrow fwhm). In conclusion, 1-octanol, a green chemical already used in food and perfume industries, is suggested as a functional additive to tune the particle size and to adjust spectral properties of the colloidal quaternary ZnCdSSe/ZnS nanocrystals.

## ■ ASSOCIATED CONTENT

### Supporting Information

The Supporting Information is available free of charge at https://pubs.acs.org/doi/10.1021/acs.jpcc.1c01676.

Equations of lifetime, radiative and nonradiative rate constants, and dislocation density and Scherrer equation; additional $^1$H NMR spectra of TOP-HP, TOP-LP, and 1-octanol added TOP-HP; size distribution obtained by SAXS analysis; absorption and PL spectra of octanol and octanethiol added ZnCdSSe/ZnS nanocrystals; detailed table of lifetime values including decay times and relative amplitudes, absolute quantum yields, and calculated rate constant; several images of defect structures of ZnCdSSe/ZnS nanocrystals due to the 1-octanol addition (PDF)

## ■ AUTHOR INFORMATION


### Corresponding Author

**Serdar Özçelik** − *Department of Chemistry, Izmir Institute of Technology, Urla 35430, İzmir, Turkey;* orcid.org/0000-0003-2029-0108; Phone: +90 232 750 75 57; Email: serdarozcelik@iyte.edu.tr

### Authors

**Seçil Sevim Ünlütürk** − *Department of Chemistry, Izmir Institute of Technology, Urla 35430, İzmir, Turkey;* Present Address: S.S.Ü.: Micro-Electro-Mechanical Systems Research and Application Center (METU-MEMS), Middle East Technical University, Çankaya, 06530 Ankara, Turkey.; orcid.org/0000-0001-8300-3837

**Ali Çağır** − *Department of Chemistry, Izmir Institute of Technology, Urla 35430, İzmir, Turkey;* orcid.org/0000-0003-0347-6656

**Canan Varlıklı** − *Department of Photonics, Izmir Institute of Technology, Urla 35430, İzmir, Turkey;* orcid.org/0000-0002-1081-0803

Complete contact information is available at: https://pubs.acs.org/10.1021/acs.jpcc.1c01676


### Author Contributions

The manuscript was written through the contributions of all authors.

### Notes

The authors declare no competing financial interest.

## ■ ACKNOWLEDGMENTS

This work was supported by Grant 115F616 from the Scientific and Technological Research Council of Turkey (TUBITAK). We thank Dr. Aziz Genç for TEM measurements and valuable discussions regarding structural analysis, and Prof. Dr. Servet Turan and Dr. Umut Savacı for TEM measurements.

## ■ REFERENCES


(1) Murray, C. B.; Norris, D. J.; Bawendi, M. G. Synthesis and characterization of nearly monodisperse CdE (E = sulfur, selenium, tellurium) semiconductor nanocrystallites. *J. Am. Chem. Soc.* **1993**, *115*, 8706−8715.

(2) Peng, X.; Wickham, J.; Alivisatos, A. P. Kinetics of II-VI and III-V Colloidal Semiconductor Nanocrystal Growth:"Focusing" of Size Distributions. *J. Am. Chem. Soc.* **1998**, *120*, 5343−5344.

(3) Zhou, J.; Liu, Y.; Tang, J.; Tang, W. Surface ligands engineering of semiconductor quantum dots for chemosensory and biological applications. *Mater. Today* **2017**, *20*, 360−376.

(4) Chandan, H. R.; Saravanan, V.; Pai, R. K.; Balakrishna, R. G. Synergistic effect of binary ligands on nucleation and growth/size effect of nanocrystals: Studies on reusability of the solvent. *J. Mater. Res.* **2014**, *29*, 1556−1564.

(5) Morris-Cohen, A. J.; Donakowski, M. D.; Knowles, K. E.; Weiss, E. A. The Effect of a Common Purification Procedure on the Chemical Composition of the Surfaces of CdSe Quantum Dots Synthesized with Trioctylphosphine Oxide. *J. Phys. Chem. C* **2010**, *114*, 897−906.

(6) Morris-Cohen, A. J.; Frederick, M. T.; Lilly, G. D.; McArthur, E. A.; Weiss, E. A. Organic Surfactant-Controlled Composition of the Surfaces of CdSe Quantum Dots. *J. Phys. Chem. Lett.* **2010**, *1*, 1078−1081.

(7) Gao, Y.; Peng, X. Crystal Structure Control of CdSe Nanocrystals in Growth and Nucleation: Dominating Effects of Surface versus Interior Structure. *J. Am. Chem. Soc.* **2014**, *136*, 6724−6732.

(8) Wang, F.; Tang, R.; Kao, J. L. F.; Dingman, S. D.; Buhro, W. E. Spectroscopic Identification of Tri-n-octylphosphine Oxide (TOPO) Impurities and Elucidation of Their Roles in Cadmium Selenide Quantum-Wire Growth. *J. Am. Chem. Soc.* **2009**, *131*, 4983−4994.

(9) Kanaras, A. G.; Sönnichsen, C.; Liu, H.; Alivisatos, A. P. Controlled Synthesis of Hyperbranched Inorganic Nanocrystals with Rich Three-Dimensional Structures. *Nano Lett.* **2005**, *5*, 2164−2167.

(10) Wang, F.; Tang, R.; Buhro, W. E. The Trouble with TOPO; Identification of Adventitious Impurities Beneficial to the Growth of Cadmium Selenide Quantum Dots, Rods, and Wires. *Nano Lett.* **2008**, *8*, 3521−3524.

(11) Peng, X.; Manna, L.; Yang, W.; Wickham, J.; Scher, E.; Kadavanich, A.; Alivisatos, A. P. Shape control of CdSe nanocrystals. *Nature* **2000**, *404*, 59−61.

(12) Kopping, J. T.; Patten, T. E. Identification of Acidic Phosphorus-Containing Ligands Involved in the Surface Chemistry of CdSe Nanoparticles Prepared in Tri-N-octylphosphine Oxide Solvents. *J. Am. Chem. Soc.* **2008**, *130*, 5689−5698.

(13) Knittel, F.; Gravel, E.; Cassette, E.; Pons, T.; Pillon, F.; Dubertret, B.; Doris, E. On the Characterization of the Surface Chemistry of Quantum Dots. *Nano Lett.* **2013**, *13*, 5075−5078.

(14) Anderson, N. C.; Owen, J. S. Soluble, Chloride-Terminated CdSe Nanocrystals: Ligand Exchange Monitored by 1H and 31P NMR Spectroscopy. *Chem. Mater.* **2013**, *25*, 69−76.

(15) Hens, Z.; Martins, J. C. A Solution NMR Toolbox for Characterizing the Surface Chemistry of Colloidal Nanocrystals. *Chem. Mater.* **2013**, *25*, 1211−1221.

(16) Gomes, R.; Hassinen, A.; Szczygiel, A.; Zhao, Q.; Vantomme, A.; Martins, J. C.; Hens, Z. Binding of Phosphonic Acids to CdSe Quantum Dots: A Solution NMR Study. *J. Phys. Chem. Lett.* **2011**, *2*, 145−152.

(17) Kalyuzhny, G.; Murray, R. W. Ligand Effects on Optical Properties of CdSe Nanocrystals. *J. Phys. Chem. B* **2005**, *109*, 7012−7021.

(18) Bonilla, C. A. M.; Flórez, M.-H. T.; Molina Velasco, D. R.; Kouznetsov, V. V. Surface characterization of thiol ligands on CdTe quantum dots: analysis by 1H NMR and DOSY. *New J. Chem.* **2019**, *43*, 8452−8458.

(19) Harris, R. D.; Amin, V. A.; Lau, B.; Weiss, E. A. Role of Interligand Coupling in Determining the Interfacial Electronic Structure of Colloidal CdS Quantum Dots. *ACS Nano* **2016**, *10*, 1395−1403.

(20) Jin, S.; Harris, R. D.; Lau, B.; Aruda, K. O.; Amin, V. A.; Weiss, E. A. Enhanced Rate of Radiative Decay in CdSe Quantum Dots upon

Adsorption of an Exciton-Delocalizing Ligand. *Nano Lett.* **2014**, *14*, 5323−5328.
(21) Jin, H.; Goryca, M.; Janicke, M. T.; Crooker, S. A.; Klimov, V. I. Exploiting Functional Impurities for Fast and Efficient Incorporation of Manganese into Quantum Dots. *J. Am. Chem. Soc.* **2020**, *142*, 18160−18173.
(22) Lee, K.-H.; Han, C.-Y.; Kang, H.-D.; Ko, H.; Lee, C.; Lee, J.; Myoung, N.; Yim, S.-Y.; Yang, H. Highly Efficient, Color-Reproducible Full-Color Electroluminescent Devices Based on Red/Green/Blue Quantum Dot-Mixed Multilayer. *ACS Nano* **2015**, *9*, 10941−10949.
(23) Fisher, A. A. E.; Osborne, M. A.; Day, I. J.; Lucena Alcalde, G. Measurement of ligand coverage on cadmium selenide nanocrystals and its influence on dielectric dependent photoluminescence intermittency. *Commun. Chem.* **2019**, *2*, 63.
(24) Wang, W.; Banerjee, S.; Jia, S.; Steigerwald, M. L.; Herman, I. P. Ligand Control of Growth, Morphology, and Capping Structure of Colloidal CdSe Nanorods. *Chem. Mater.* **2007**, *19*, 2573−2580.
(25) Smith, A. M.; Nie, S. Semiconductor nanocrystals: structure, properties, and band gap engineering. *Acc. Chem. Res.* **2010**, *43*, 190−200.
(26) Bailey, R. E.; Nie, S. Alloyed Semiconductor Quantum Dots: Tuning the Optical Properties without Changing the Particle Size. *J. Am. Chem. Soc.* **2003**, *125*, 7100−7106.
(27) Yarema, O.; Yarema, M.; Wood, V. Tuning the Composition of Multicomponent Semiconductor Nanocrystals: The Case of I-III-VI Materials. *Chem. Mater.* **2018**, *30*, 1446−1461.
(28) Riehle, F. S.; Yu, K. Role of Alcohol in the Synthesis of CdS Quantum Dots. *Chem. Mater.* **2020**, *32*, 1430−1438.
(29) Qu, L.; Peng, Z. A.; Peng, X. Alternative Routes toward High Quality CdSe Nanocrystals. *Nano Lett.* **2001**, *1*, 333−337.
(30) Arndt, D.; Thöming, J.; Bäumer, M. Improving the quality of nanoparticle production by using a new biphasic synthesis in a slug flow microreactor. *Chem. Eng. J.* **2013**, *228*, 1083−1091.
(31) Keating, M.; Chen, Y.; Larmour, I. A.; Faulds, K.; Graham, D. Growth and surface-enhanced Raman scattering of Ag nanoparticle assembly in agarose gel. *Meas. Sci. Technol.* **2012**, *23*, 084006.
(32) Shrestha, A.; Spooner, N. A.; Qiao, S. Z.; Dai, S. Mechanistic insight into the nucleation and growth of oleic acid capped lead sulphide quantum dots. *Phys. Chem. Chem. Phys.* **2016**, *18*, 14055−14062.
(33) Zhang, C.; Xia, Y.; Zhang, Z.; Huang, Z.; Lian, L.; Miao, X.; Zhang, D.; Beard, M. C.; Zhang, J. Combination of Cation Exchange and Quantized Ostwald Ripening for Controlling Size Distribution of Lead Chalcogenide Quantum Dots. *Chem. Mater.* **2017**, *29*, 3615−3622.
(34) Wang, X.; Qu, L.; Zhang, J.; Peng, X.; Xiao, M. Surface-Related Emission in Highly Luminescent CdSe Quantum Dots. *Nano Lett.* **2003**, *3*, 1103−1106.
(35) Wu, F.; Zhang, J. Z.; Kho, R.; Mehra, R. K. Radiative and nonradiative lifetimes of band edge states and deep trap states of CdS nanoparticles determined by time-correlated single photon counting. *Chem. Phys. Lett.* **2000**, *330*, 237−242.
(36) Sadhu, S.; Patra, A. Lattice Strain Controls the Carrier Relaxation Dynamics in CdxZn1-xS Alloy Quantum Dots. *J. Phys. Chem. C* **2012**, *116*, 15167−15173.
(37) Omogo, B.; Aldana, J. F.; Heyes, C. D. Radiative and Non-Radiative Lifetime Engineering of Quantum Dots in Multiple Solvents by Surface Atom Stoichiometry and Ligands. *J. Phys. Chem. C* **2013**, *117*, 2317−2327.
(38) Maksimov, M. V.; Sizov, D. S.; Makarov, A. G.; Kayander, I. N.; Asryan, L. V.; Zhukov, A. E.; Ustinov, V. M.; Cherkashin, N. A.; Bert, N. A.; Ledentsov, D.; et al. Effect of nonradiative recombination centers on photoluminescence efficiency in quantum dot structures. *Semiconductors* **2004**, *38*, 1207−1211.
(39) Ramasamy, V.; Mohana, V.; Rajendran, V. Characterization of Ca doped CeO2 quantum dots and their applications in photo-catalytic degradation. *OpenNano* **2018**, *3*, 38−47.
(40) He, K.; Chen, N.; Wang, C.; Wei, L.; Chen, J. Method for Determining Crystal Grain Size by X-Ray Diffraction. *Cryst. Res. Technol.* **2018**, *53*, 1700157.


https://doi.org/10.1021/acs.jpcc.1c01676
J. Phys. Chem. C 2021, 125, 14401−14408